

1                   **Analysis of hydrogen adsorption and surface binding configuration on**  
2                   **tungsten using direct recoil spectroscopy**

3                   R. D. Kolasinski<sup>\*,(a)</sup>, K. Hammond<sup>(b)</sup>, J. A. Whaley<sup>(a)</sup>, D. A. Buchenauer<sup>(a)</sup>, and B. D.  
4                   Wirth<sup>(b)</sup>

5                   <sup>(a)</sup>*Sandia National Laboratories, Hydrogen and Metallurgical Science Department, Livermore,*  
6                   *CA 94551 USA*

7                   <sup>(b)</sup>*University of Tennessee, Department of Nuclear Engineering, Knoxville, TN 37996 USA*

8  
9                   ***Abstract*** – In this work, we apply low energy ion beam analysis to directly examine how the  
10                  adsorbed hydrogen concentration and binding configuration on W(100) depend on temperature. We  
11                  exposed the tungsten surface to fluxes of both atomic and molecular H and D. Using 1-2 keV Ne<sup>+</sup> ions,  
12                  we then probed the H isotopes adsorbed along different crystallographic directions. At saturation  
13                  coverage, H occupies two-fold bridge sites on W(100) at 25 °C. The H surface coverage dramatically  
14                  changes the behavior of channeled ions along the surface, as does reconstruction of the surface W  
15                  atoms. For the exposure conditions examined here, we found that surface sites remain populated with  
16                  H until the surface temperature reaches 200 °C. After this point, we observe H rapidly desorbing until  
17                  only a residual concentration remains at 450 °C. Development of an efficient molecular dynamics  
18                  algorithm that accurately reproduces the experimental ion energy spectra and azimuthal variation of  
19                  recoiled H is underway.

20                  PACS codes: 68.43.Fg, 68.49.Sf, 34.50.-s, 61.85.+p

21                  PSI-21 keywords: ion-surface collisions, hydrogen recycling, hydrogen adsorption, molecular  
22                  dynamics simulations, tungsten

23

24                  Corresponding author address:

25

26                  Robert D. Kolasinski  
27                  Sandia National Laboratories  
28                  P.O. Box 969, MS 9161  
29                  Livermore, CA 94550 USA  
30                  e-mail: rkolasi@sandia.gov

31

32

33

34 **I. Introduction**

35 Adsorption, recombination, and exchange of hydrogen isotopes on surfaces are of fundamental  
36 interest from the perspective of recycling from plasma-facing materials in magnetic fusion devices.  
37 The atomic-scale details of these processes are difficult to resolve experimentally, largely because  
38 most surface analysis techniques cannot detect adsorbed hydrogen. Two exceptions include low  
39 energy ion scattering (LEIS) and direct recoil spectroscopy (DRS), both of which provide *direct*  
40 information on the adsorbed hydrogen configuration on surfaces, as well as binding energies and  
41 exchange kinetics. Such insight complements ongoing fundamental atomic-scale modelling efforts  
42 (e.g. density functional theory or molecular dynamics) that focus on simulating the complex chemical  
43 effects that occur when surfaces are exposed to high flux plasmas. Experiments are needed to strongly  
44 test these models, thereby motivating further refinements to interatomic potentials and other  
45 simulation inputs.

46 Both LEIS and DRS are forms of low energy ion beam analysis which provide both composition  
47 and structural information, with high surface-specificity (< 1nm sampling depth.) In terms of the  
48 underlying physics, these techniques bear many similarities to their higher energy counterparts,  
49 Rutherford backscattering spectroscopy and elastic recoil detection. We refer the reader to several  
50 excellent reviews [1,2] for further details. In our prior work, we used LEIS and DRS to study the  
51 hydrogen binding configuration along open channels on the W(100) crystal plane [3]. While we were  
52 able to definitively identify two-fold bridge sites as the preferred binding site for complete coverage  
53 of the W surface with hydrogen, the details of the binding configuration at lower coverage were still  
54 unclear. Furthermore, the equilibrium surface coverage as a function of temperature was left  
55 unaddressed in our prior work. While this could be inferred from the H evolved from the surface  
56 during thermal desorption, DRS provides a direct measure. This coverage dependence is somewhat  
57 complicated due to reconstruction of the surface as the adsorbed H desorbs, where W surface atoms  
58 are displaced out of ideal bulk-terminated sites.

59 With the above concerns in mind, we address the temperature/coverage effects in greater detail in  
60 the present study. We use ion focusing along surface channels as a sensitive means of determining the  
61 hydrogen concentration present on the surface. To calibrate this process, we dosed the surface with  
62 both atomic and molecular H and D, and measured the recoiled adsorbate signals as a function of  
63 temperature under a variety of conditions, with the goal of comparing our results with recently-  
64 developed models of surface adsorption/recombination kinetics [4].

65 To complement our experimental results, we are developing an MD model to simulate H  
66 migration on the W(100) surface. The use of MD allows for the inclusion of more sophisticated  
67 potentials and provides a more realistic calculation of interatomic forces than possible with the binary  
68 collision approximation (BCA) models that are frequently used as inputs to recycling codes. For the  
69 purpose of modeling the LEIS/DRS experiments, we also developed an MD framework to simulate  
70  $\text{Ne}^+$  scattering on the crystal surface.

## 71 **II. Experiment**

72 Our scattering experiments were performed using an ion energy spectrometer, which has been  
73 previously described in Ref. [5]. Briefly, the system includes an ion source that produces mass-  
74 separated beams through electron bombardment of inert gases. Scattered or recoiled particles are  
75 detected with a hemispherical analyzer (50 mm radius) with a  $2^\circ$  acceptance angle. For this set of  
76 measurements, we used beams of low energy (1 keV and 2 keV)  $\text{Ne}^+$  ions to characterize a 7 mm dia.,  
77 1 mm thick W single crystal (MaTecK GmbH) that had been polished and aligned to within  $0.1^\circ$  of  
78 the (001) plane. We secured the crystal with Ta wire along its outer circumference to a button-style  
79 heater and an isolating sapphire disc. A well-ordered, clean sample surface could be achieved through  
80 repeated cycles of sputtering with 2 keV  $\text{Ne}^+$  ions at grazing incidence followed by heating to 450 °C.  
81 The  $\text{Ne}^+$  ion beam (100 nA current) was rastered over a 2 mm  $\times$  2 mm area, producing an incident  
82 flux of  $1.5 \times 10^{13} \text{ cm}^{-2} \text{s}^{-1}$ . The raster amplitude was adjusted with incidence angle to maintain a  
83 constant spot size and flux on the sample surface.

84 The concentration of hydrogen isotopes on the W crystal surface could be controlled by varying  
85 the surface temperature or the incident flux of hydrogen isotopes. For the purposes of dosing, we  
86 introduced the hydrogen through a 1 mm ID tungsten capillary into our vacuum system. The tungsten  
87 capillary could be heated by electron bombardment to 1700 °C to allow for complete dissociation of  
88 the effusing hydrogen flux, thus allowing us to dose with either atomic or molecular species.

89 The key geometrical parameters for this set of experiments are illustrated in Fig. 1(a), including  
90 the angle of incidence of the analysis beam ( $\alpha$ ), the azimuth on the W(100) surface ( $\phi$ ), and  
91 observation angle ( $\theta$ ). Recall that the energies of the scattered and recoiled particles are used to  
92 identify species present on the surface. Consider Fig. 1(b), which shows ion energy spectra for 2 keV  
93  $\text{Ne}^+ \rightarrow \text{W}(100)$  in cases where the surface is exposed to background gases present within the vacuum  
94 system only, as well as during exposure to  $\text{D}_2(\text{g})$ . Note that we have normalized all energies relative to  
95 that of the incident beam ( $E_0$ ). Within the two spectra, three prominent peaks are readily visible,  
96 corresponding to H, D, and W present on the surface. The vertical lines indicate the theoretical  
97 positions for these peaks, calculated using classical kinematics and ignoring any inelastic energy loss  
98 mechanisms. Even when the surface is not dosed, a peak associated with recoiled H is still present,  
99 which we attribute to dissociative chemisorption of residual  $\text{H}_2(\text{g})$  present in our vacuum system.  
100 Hydrogen in dissolved within the W lattice may also diffuse to the surface, although this is expected  
101 to be only a minor contribution to the H surface concentration.

102 Once the surface was exposed to  $\text{D}_2(\text{g})$ , the signals associated with W and H rapidly diminished.  
103 We systematically tested different molecular fluxes to the surface, finding that saturation coverage at  
104 25 °C could be assured with a partial pressure of  $3.0 \times 10^{-7}$  torr. This concentration depends on a  
105 dynamic equilibrium dictated by the arrival rate of  $\text{H}_2(\text{g})$ , the sticking and reflection coefficients, as  
106 well as the desorption rate due recombination. One key concern is that the incident ion beam used for  
107 our measurements also contributes to desorption. To minimize this effect, we ensured that the  
108 exposure flux produced an arrival rate of  $\text{H}_2(\text{g})$  at the surface was much higher than that of the  
109 incident  $\text{Ne}^+$  ions. Based on the kinetic theory of gases, the aforementioned partial pressure of  $3.0 \times 10^{-7}$   
110 torr corresponds to a flux of  $3.0 \times 10^{14} \text{ D}_2 \text{ cm}^{-2} \text{ s}^{-1}$ , or a factor of 20 higher than the ion arrival rate at

111 the surface. In practice, because the gas is directed toward the sample through a W capillary, its  
112 arrival rate at the sample surface is much higher.

113 We were able to calculate the chemisorbed concentrations of H and D by integrating the area  
114 under each peak and correcting the result for the recoil cross-sections for each species. For 2 keV  $\text{Ne}^+$   
115 and a laboratory recoil angle of  $\theta=25^\circ$ , the relevant cross-sections are:  $5.93 \times 10^{-2} \text{ \AA}^2/\text{sr}$  (H) and  
116  $2.96 \times 10^{-2} \text{ \AA}^2/\text{sr}$  (D). Assuming that the dosed case shown in Fig. 1(b) corresponds to a saturation  
117 coverage of hydrogen isotopes, the H coverage is 6%, with the remaining D comprising 94% of the  
118 total.

119 **III. Coverage as a function of temperature**

120 To better understand the coverage dependence as a function of temperature, we performed a  
121 systematic series of controlled adsorption experiments, in a manner similar to the procedures specified  
122 in Ref. [4]. This involved rapidly heating the crystal to 450 °C while exposing the sample to different  
123 fluxes of deuterium or hydrogen. In each case, the sample was held at 450 °C for 30 min and then  
124 allowed to cool at a linear rate of 7.1 °C/min. During the entire process, we monitored the recoiled  
125 peak height corresponding to hydrogen isotopes adsorbed on the surface. We obtained all  
126 measurements using a 2 keV  $\text{Ne}^+$  beam at an incidence angle of  $\alpha=80^\circ$  to probe the hydrogen present  
127 along the <100> surface direction.

128 In Fig. 2, we show recoil signals from D adsorbed on the W(100) surface as the temperature is  
129 slowly cooled from 450 °C using the procedure described above. In case (a), different D exposure  
130 pressures are considered, ranging over an order of magnitude between  $p=7.4 \times 10^{-8}$  torr to  $1.1 \times 10^{-6}$  torr.  
131 To aid in the interpretation of the data, we render the adsorption curves as Arrhenius plots. In addition,  
132 we assume that once the surface temperature declined below 100 °C the surface was saturated with H  
133 or D, hence the curves to this saturation condition. Keep in mind that the sampling depth of our  
134 analysis beam at oblique incidence is <1 nm, hence all signals shown here correspond to H present on  
135 the surface. Regardless of the exposure pressure, the same basic adsorption curve shape is evident. In  
136 the Arrhenius coordinates, the adsorbed concentrations follow a nearly linear dependence until the

137 temperature approaches 300 °C. Afterward, the adsorption rate slows until it reaches a constant level  
138 for  $T > 150$  °C. As shown in case (a), modifying the exposure pressure offsets the adsorption profile  
139 along the  $1/T$  axis without affecting its slope.

140 It was also of interest to if dosing the samples with atomic D versus D<sub>2</sub> would produce any  
141 appreciable result in the adsorbed concentrations on the surface. Adsorption curves for both cases are  
142 shown in Fig. 2(b). We could not discern an appreciable difference within the error of our experiment.  
143 We also noted a slight offset between chemisorption of H<sub>2</sub> and D<sub>2</sub> adsorption on the surface, but the  
144 difference was very slight and still within the error of our experiment. This indicates that any  
145 dependence of adsorption on isotope is rather modest.

146 **IV. Variation of binding configuration as a function of temperature**

147 For single crystal surfaces, it is possible to use LEIS and DRS to gain detailed information about  
148 the structure of surfaces. The main effect exploited here is surface channeling. At grazing angles of  
149 incidence, the energy of the incoming Ne<sup>+</sup> particles perpendicular to the sample surface is very small,  
150 enabling the tungsten substrate atoms to gently deflect them along open channels on the crystal  
151 surface. For W(100), the predominant channels are along the <100> and <110> directions, as  
152 illustrated by the shaded regions in Fig. 3. Ion focusing increases the likelihood of collisions between  
153 the incident Ne<sup>+</sup> and any adsorbed H bound along a given channel. Hence, enhanced signals from  
154 recoiled hydrogen would be observed along surface channels containing hydrogen, thereby enabling a  
155 definitive identification of the binding configuration. More details on the use of surface channeling to  
156 study adsorbed H may be found in Ref. [3].

157 To aid in our analysis of the adsorbed H layer, we monitored recoiled H peak height over a wide  
158 range of incidence angles ( $\alpha$ ) and azimuths ( $\phi$ ). These data are compiled into the maps depicted in Fig.  
159 4. To examine the binding configuration as a function of temperature (and surface H coverage), we  
160 considered four different temperatures between 25 °C and 350 °C, as shown in cases (a-d). All of the  
161 maps were acquired at an observation angle of  $\theta=45^\circ$  using 1 keV Ne<sup>+</sup>; in each case we exposed the  
162 surface to a H<sub>2</sub> partial pressure of  $3\times10^{-7}$  torr. Immediately evident in each map is the presence of

163 distinct hydrogen recoil structures along the <100> and <110> directions that repeat every 90°,  
164 annotated respectively by “A” and “B” in Fig. 4. The slight variability in the repeating pattern with  
165 azimuth is due to a small misalignment of the crystal surface normal with respect to the incident beam.

166 The saturation coverage case at 25 °C depicted in Fig. 4(a) is nearly identical to our prior  
167 observations described in Ref. [1], with the same distinct hydrogen recoil patterns aligned along the  
168 <100> and <110> directions. This pattern provides clear evidence of adsorbed H residing in 2-fold  
169 (bridge) sites on the W(100) surface at 25 °C at saturation coverage. Had the hydrogen been residing  
170 other high symmetry surface sites (such as four-fold hollow or top), recoiled hydrogen would not be  
171 observed along both the <100> and <110> azimuths. In addition, prior low energy electron diffraction  
172 (LEED) measurements provide compelling evidence that at 25 °C, the W surface atoms on the (100)  
173 plane reside in a 1×1 configuration when saturated with hydrogen [7,8]. This configuration is  
174 illustrated in Fig. 3(a), and corresponds to 2 H/W (or  $2 \times 10^{15}$  H/cm<sup>2</sup>). Note that the dashed line in this  
175 figure indicates the surface unit cell.

176 Our previous analysis described in Ref. [1] did not reveal the definitive binding configuration at  
177 partial coverage. (In the present study, the carefully controlled H dosing and systematic examination  
178 of coverage with temperature provided an opportunity for further analysis.) The surface behavior  
179 under these conditions becomes more complex, as the aforementioned LEED measurements indicate  
180 that the W surface atoms displace laterally by 0.2 Å to form a *c*(2×2)+H surface reconstruction, as  
181 depicted in Fig. 3(b). The positions of the tungsten surface atoms are crucial, as they affect both the  
182 adsorbed hydrogen configuration as well as how ions are scattered along the surface. In the  
183 reconstructed configuration, the surface channels along the <100> directions narrow by 0.4 Å (by  
184 13 %). While the positions of the W surface atoms can easily be detected by LEED, the relative  
185 positions of the H adatoms cannot be determined with this approach.

186 At 150 °C, the intensity patterns along the <100> and <110> directions still persist, indicating that  
187 bridge sites are still preferred, even at lower coverage. The H recoil patterns, however, subtend a  
188 smaller azimuthal range than is evident in the saturation coverage case. This behavior is consistent

189 with narrowing of the surface channels on the reconstructed surface. At 250 °C and higher, the same  
190 basic recoil pattern persists, thereby confirming that H remains in bridge sites even at low coverage.

191 **V. Model Development and Summary**

192 While the analysis discussed presented here provides support for bridge site occupation for all  
193 coverage on W(100), a more compelling case can be made through computational modeling of surface  
194 collisions. Because grazing incidence angles are used to probe the tungsten surface, the incident ions  
195 interact with many surface atoms at once. The computational approach that most closely simulates  
196 this is molecular dynamics (MD). While MD simulations are often considered impractical for  
197 simulating scattering, simplifying assumptions (as discussed in Ref. [9]) can be readily incorporated  
198 to make the problem more tractable. Using LAMMPS, we are developing simulations of ion  
199 scattering at grazing incidence along the <100> and <110> surface channels, while varying the  
200 amount of H present to match the measured surface coverage.

201 A key starting point for this work involves the evaluation of interatomic potentials for  
202 incorporation into MD simulations. Since most potentials are optimized to reproduce bulk properties,  
203 surface properties may not be well represented. Such problems aside, we do not foresee any  
204 insurmountable obstacles to applying MD techniques to the scattering analyses presented here. The  
205 coupling of such experiments and models provides an promising avenue for validating models of  
206 atomic-scale phenomenon of interest to ITER and beyond.

207 **VI. Acknowledgements**

208 We thank Thomas Felter and Robert Bastasz for helpful discussions regarding this work. Sandia  
209 National Laboratories is a multi-program laboratory managed and operated by Sandia Corporation, a  
210 wholly owned subsidiary of Lockheed Martin Corporation, for the U.S. Department of Energy's  
211 National Nuclear Security Administration under contract DE-AC04-94AL85000.

212 **References**

213 [1] R. Bastasz and W. Eckstein, Particle Scattering, in: E. N. Kaufmann (Ed.), *Characterization of*  
214 *Materials*, John Wiley & Sons, Inc., 2012, 1-16.

215 [2] H. Niehus, W. Heiland, and E. Taglauer, *Surf. Sci. Rep.*, **17** (1993) 213.

216 [3] R. D. Kolasinski, N. C. Bartelt, J. A. Whaley, and T. E. Felter, *Phys. Rev. B*, **85** (2012) 115422.

217 [4] S. Markelj, O. Ogorodnikova, P. Pelicon, T. Schwarz-Selinger, and I. Čadež, *Appl. Surf. Sci.*, **282**  
218 (2013) 478.

219 [5] R. Bastasz, J. A. Whaley, T. A. Lograsso, and C. J. Jenks, *Philos. Mag.*, **86** (2006) 855.

220 [6] T. Schwarz-Selinger, A. von Keudell, and W. Jacob, *J. Vac. Sci. Technol. A*, **18** (2000) 995.

221 [7] R. A. Barker and P. J. Estrup, *Phys. Rev. Lett.* **41** (1978) 1307.

222 [8] D. A. King, *Phys. Scr.* **T4** (1983) 34.

223 [9] D. Danailov, D. J. O'Connor, K. J. Snowdon, *Surf. Sci.* **347** (1996) 215.

224

225 **Figure Captions**

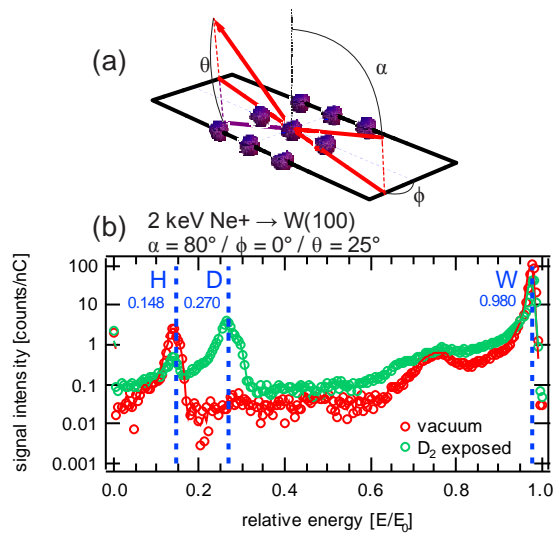
226 FIG. 1: (a) Illustration of scattering geometry showing definitions of the polar ( $\alpha$ ), azimuthal ( $\phi$ ), and  
227 observation ( $\theta$ ) angles. (b) Ion energy spectra for scattered Ne and recoiled H and D from the W(100)  
228 surface. Dashed lines correspond to calculated elastic scattering and recoil energies for the indicated  
229 surface species.

230 FIG. 2: Adsorption profiles for hydrogen isotopes on W(100). Case (a) shows the dependence on D<sub>2</sub>(g)  
231 exposure pressure, whereas case (b) compares adsorption of different isotopes and illustrates the  
232 effect of dosing with atomic species.

233 FIG. 3: Hydrogen configuration on W(100) at (a) saturation coverage, and (b) partial coverage. Large  
234 markers indicate W surface atoms, small markers indicate adsorbed H. Prominent channeling  
235 directions are indicated by the shaded regions, and the surface unit cell is indicated by the dashed line.

236 FIG. 4: Ion scattering maps depicting H recoiled from the W(100) surface, for four different surface  
237 temperatures. Experimental conditions: H<sub>2</sub>(g) partial pressure of  $3 \times 10^{-7}$  torr;  $\theta=45^\circ$ .

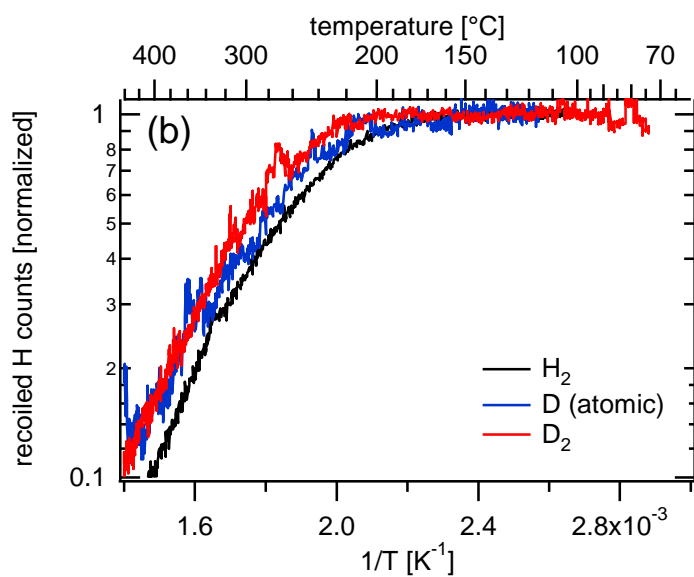
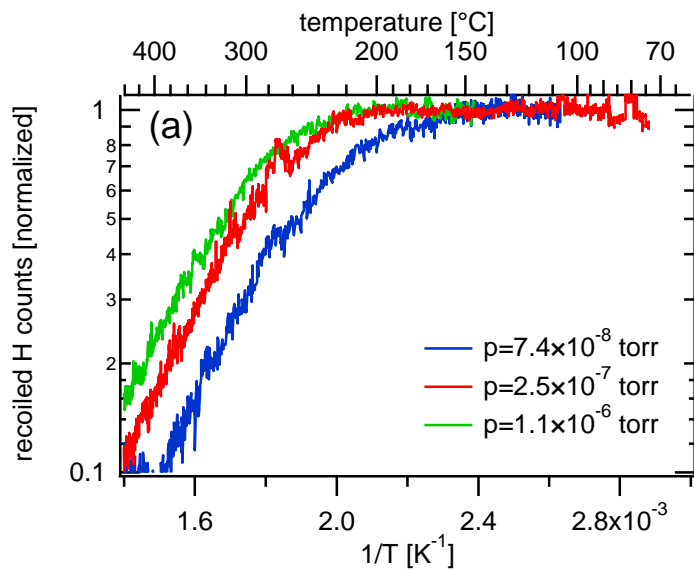
238



239

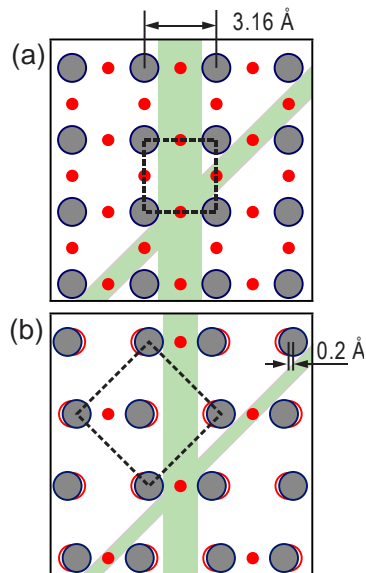
240 FIG. 1

241



244 FIG. 2

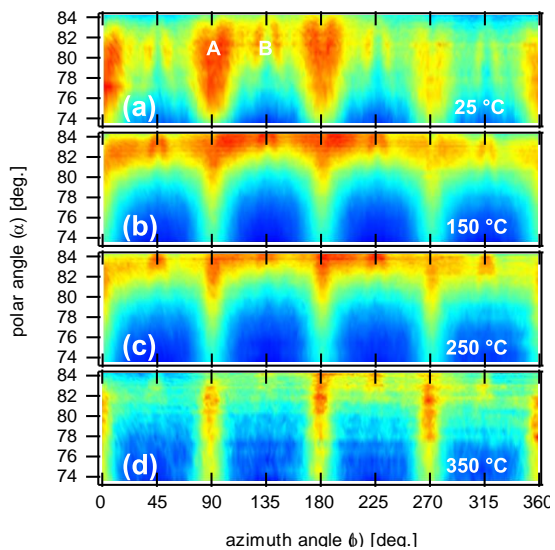
245



246

247 FIG. 3

248



249

250 FIG. 4